Separation and Purification Technology 377 (2025) 134230

Contents lists available at ScienceDirect

Separation and Purification Technology

journal homepage: www.elsevier.com/locate/seppur

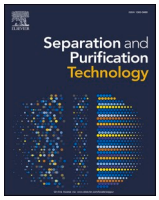

Development of a dynamic process model for the mechanical fluid separation in disk stack centrifuges

Helene Katharina Baust [a], Zihim Lam [b], Michael Hay [b], Hermann Nirschl [a], Marco Gleiß [a,*]

[a] Institute of Mechanical Process Engineering and Mechanics, Karlsruhe Institute of Technology, Straße am Forum 8, 76131 Karlsruhe, Germany
[b] Process Technology & Engineering, Evonik Operations GmbH, Rodenbacher Chaussee 4, 63457 Hanau-Wolfgang, Germany

ARTICLE INFO

Editor: V. Tarabara

Keywords:
Centrifuge
Solid-liquid separation
Disk stack centrifuge
Dynamic process model
Digitization
Real-time modeling
Material characterization

ABSTRACT

This work presents an innovative process model that simulates the dynamic separation processes in disk stack centrifuges. Current process simulation tools for the calculation of the separation process in disk stack centrifuges are limited to steady-state conditions and are not suitable for real-time simulations. A physically based computational model has been developed that combines experimentally derived material functions with dynamic modeling. The material functions represent the physical behavior such as sedimentation and sediment formation within the apparatus that are relevant to calculate separation. The dynamic model is based on a partitioning of the process area into individual compartments and this describes the transient behavior of the apparatus. The numerical algorithm presented is able to map the residence time distribution of the solids in the apparatus in real time. The validation of the developed model was performed by comparing numerical simulations with experimental results.

1. Introduction

Around 60 % of the products of the chemical industry are polymeric, crystalline or amorphous solids [1]. Thereby, an essential basic operation is the mechanical fluid separation of dispersed particles from a continuous liquid phase. In addition to the chemical industry, mechanical fluid separation plays an important role in the chemical, pharmaceutical and biotechnology industry, the food industry and in the treatment of minerals and waste water [2–12]. Centrifuges are often used at high centrifugal forces which enable the separation of fine dispersed particles or particles with a low density difference to the surrounding continuous phase. A widely used centrifuge is the disk separator, which particularly serves to clarify turbid liquids and to concentrate diluted suspensions. The separation of three phases (solid–liquid-liquid) is also possible. Disk separators have a very large clarifying area, which is higher than that of other solid bowl centrifuges. High throughput rates with low (<0.1 vol%) or highly concentrated suspensions (10 vol% to 25 vol%) enable their use in many fields, whereby the solids concentration of the feed determines the type of outlet. At the same time, disk separators have an advantage over other types of centrifuges when it comes to separating shear-sensitive products, as their design ensures a gentle acceleration of the product flow.

The choice of a centrifuge and its design is often based on the manufacturer's experience and highly simplified analytical approaches, such as the sigma theory [13–15] which expresses the separator's performance in terms of the equivalent area of a settling tank and the g-volume [16]. Many parts of the separator are inaccessible due to high rotational speeds. Brunner [13] and Gol'din [17] have developed an analytical solution for the velocity profiles and for the separation process in the disk gap of a disk stack centrifuge. In reality, the disks are separated from each other by welded-on spacers (chaulks). Brunner [18] experimentally investigated the flow conditions at the inlet, within a single gap and a for a gap with chaulks. A vortex-shaped secondary flow formed transverse to the direction of the gap, which favored the separation of very fine particles but also resuspends particles that had already been separated. Mannweiler [19] investigated the separation of seven disk gaps. The other gaps were closed and the position of the seven open gaps varied so that they were located at the bottom, middle or top of the disk stack. The investigations showed that the separation properties depend on the location, which may be due to the effective preseparation and the different inflow conditions in the outer annular ring. Based on the equivalent clarification area approach, König et al. [20] have developed an analytical model that describes the separation efficiency in disk separators for the steady state case and corresponds

* Corresponding author.
E-mail address: marco.gleiss@kit.edu (M. Gleiß).

https://doi.org/10.1016/j.seppur.2025.134230
Received 12 May 2025; Received in revised form 25 June 2025; Accepted 4 July 2025
Available online 6 July 2025
1383-5866/© 2025 The Authors. Published by Elsevier B.V. This is an open access article under the CC BY license (http://creativecommons.org/licenses/by/4.0/).

well with experimental data. The model of the equivalent clarification area, which solely considers the disk stack, was reduced by the area clogged by sediment and at the same time extended by the contribution of the distributor and the solids holding space. The resuspension of the particles already separated in the disk stack in the solids holding space and the non-uniform flow caused by the chaulks in the disk stack were also taken into account. Distributor, solids holding space, the disk stack and the resuspension were connected in series. Each domain has an individual grade efficiency, whose sum corresponds to the total grade efficiency of the separator. Additional experiments [21] with a partially transparent separator model have shown that both the flow entering the disk gaps and the return transport of the separated solids along the underside of the disks are unevenly distributed in terms of space and time. As a result, the available clarification surface is not optimally utilized. Furthermore, the experiments have shown that the resuspension of the particles plays a less significant role in the separation process.

In recent years, numerical methods such as computational fluid dynamics (CFD) and flowsheet simulation (FSS) have made a significant contribution to understanding the complex three-dimensional and mostly transient processes and have thus developed into an important tool for the analysis, design and optimization of mechanical separation processes [22]. Janoske and Piesche [23,24] calculated the grade efficiency by means of the numerical simulation of a single disk gap for low solids volume fractions and compared the simulated results with experimental data. The flow was simulated using CFD and the particle trajectories were calculated using an Euler-Lagrange method. The focus of the analysis was on the transition point between laminar and turbulent flow, whereby a significant stabilization of the flow field was achieved through the use of chaulks. Breitling et al. [25] also dealt with the single-gap model of a disk separator and investigated the transition from laminar to turbulent flow using simulations carried out with the commercial CFD software Fluent. In turbulent flow, the separation behavior deteriorates significantly and the differences between simulations and experiments increase. Zink et al. [26] used CFD simulations to show that the flow behavior in the disk separator significantly influences the separation efficiency and also the grade efficiency. In particular, a high number of disk gaps and a low rotational speed of the centrifuge caused a highly non-uniform distribution of the gap throughputs, which in turn significantly influenced the grade efficiency. In practice, the separated particles still have to pass through the outer annular gap. Böndel [27] used CFD to add particles directly at the outer radius of the disk gap. The simulation showed that particles are deflected in the axial direction by the flow in the bowl chamber, resulting in partial resuspension of the particles and thus a deterioration in separation performance.

The literature [13,17,18,23–25] mainly focuses on the single gap. However, the increasing computing capacities finally made it possible to simulate the entire apparatus: Shekhawat et al. [28] as well as Esmaeilnejad-Ahranjani and Hajimoradi [29] use CFD to support process design. Shekhawat et al. [28] simulated the separation process of the entire apparatus by means of CFD. The different phases were modeled by an Eulerian – Eulerian multiphase model. The optimal operating range for the separation of mammalian cells was determined by comparing the turbulent kinetic energy resulting from the CFD simulations with experimental data. Higher rotational speeds led to better clarification but also to higher cell damage. An increase in the volume flow improved cell lysis and productivity, but had a negligible effect on the grade efficiency. Esmaeilnejad-Ahranjani and Hajimoradi [29] simulated both a tubular bowl centrifuge and a disk separator in CFD to identify a separation apparatus for the clarification of the product. The disk separator provided a required balance between grade efficiency and product quality.

CFD simulations offer the possibility of resolving both the flow and the separation process itself in centrifuges. However, the complete calculation of the rotating two-phase flow in the separator is not yet feasible in economically justifiable computation times due to the complex geometry and the extremely small gaps. In contrast to resolved simulations, the focus of FSS tools lies on the fundamental design and operation of large process plants. The goal is to model the entire plant on a macro scale, which includes the modeling of the process behavior, sensitivity analyses, process optimization and process control [30,31]. This macroscopic level allows solely the modeling of quantities such as mass flows and particle size distributions. Thus, the challenge is to define suitable material functions that may be described by empirical parameters in order to model microscopic properties such as sedimentation, sediment structure, agglomeration or comminution. A further challenge is the abstraction of the process by dividing it into discrete domains or mechanistic models that represent the influence of different geometric properties on the process. Recently, the use of artificial intelligence has increased to eliminate deviations between the parameter-controlled FSS and reality [32,33]. In addition to the modulation of a single apparatus [32–45], FSS also enable a combination of different apparatuses and thus the modelling of an entire process chain [46,47].

For a predictive model of the separation process in centrifuges with dynamically changing operating parameters and feed material properties, it is necessary to distinguish between machine and material functions. On the one hand, the sedimentation properties of the particle system and sediment formation influence the process and are predicted by material functions. On the other hand, machine parameters such as the volume flow and the rotational speed as well as the apparatus geometry have a significant influence on the separation of particles. The approach has already been successfully applied to sedimenting centrifuges such as decanter centrifuges [39–43] and tubular bowl centrifuges [44,45].

This study presents a dynamic FSS model forecast the grade efficiency as well as the particle size distribution and the solids volume fraction of the clarified liquid and the sediment in disk separators. Due to the complex geometry, the sedimentation of the particles takes place both in the outer annular gap and in the disk gaps themselves. For this reason, it is necessary to differentiate between these two domains, but the emphasis is on the disk gap. Internally, the temporal and spatial resolution takes place via individual compartments, which contain balance equations for either the sedimentation or the sediment formation. Sedimentation and sediment formation, its compression and the transport of the separated particles are described by experimentally determined material functions. The resulting model reproduces the separation process in real time. Further experiments were conducted for validation.

2. Modeling disk stack centrifuges

The disk separator is a solid bowl centrifuge that is used for the mechanical clarification and separation of mixtures consisting of solids and liquids. It can be operated in semi-batch or continuously, depending on the solids discharge. The separation is based on the sedimentation of the specific heavier disperse phase in the specific lighter continuous phase due to the acting centrifugal force. The main components of the separator are the bowl and the disk stack inside. The disk stack consists of several conical disks which are placed on top of each other. The distance between the disks is maintained by thin welded spacers (chaulks) in the form of ribs or dots. The high number of disks and their conical shape results in an increase in the surface area available for the separation of the particles. The centrifugal force required for the separation process is induced by the rotation of the disks and the bowl. Fig. 1 shows the operating principle of the separator. The feed flows centrally into the apparatus and is gently accelerated by the distributors to the maximum rotational speed. In the outer annular gap, the product flow divides into the individual disk gaps. The separation takes place both in the outer annular gap and within the disk gaps. In the disk gaps, the particles move to the upper disk due to their higher density under the influence of the centrifugal field and are separated there. Due to the centrifugal force, the separated particles move back towards the outer

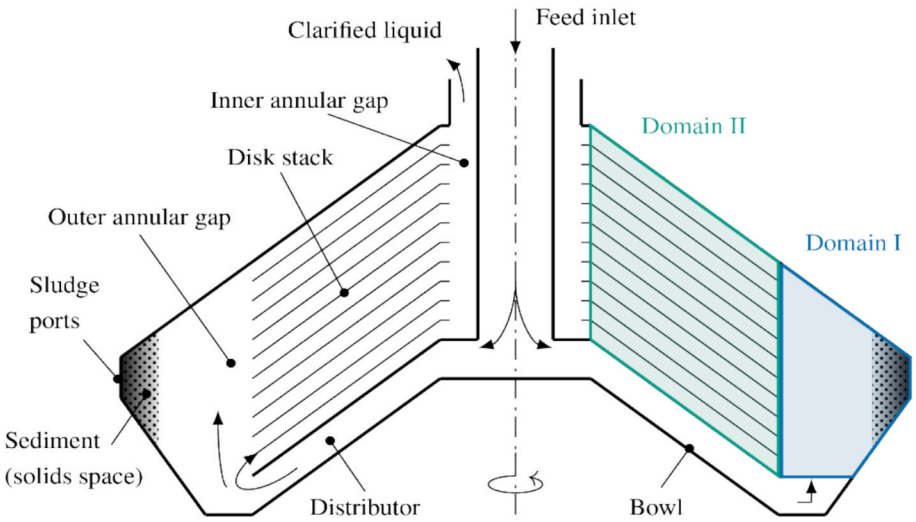

Fig. 1. Schematic illustration of the disk stack centrifuge and division of the separator into two modeling domains.

annular gap and accumulate in the sludge domain. There are different variants for the solids discharge: discontinuous (manual removal of the separated solids), semi-continuous (periodic opening of the sludge ports for emptying) or completely continuous (nozzle separator). Meanwhile, the clarified liquid flows from the disk stack into the inner annular gap and leaves the apparatus from there.

To record the overall behavior of the separation process in disk separators, it is necessary to consider all relevant separation processes. For this purpose, the apparatus was divided into two domains (Fig. 1). The inlet and outlet geometry are neglected, solely the domains in which separation takes place are taken into account. Fig. 2 shows all mass flows of the two domains. In domain I, the liquid enters the outer annular gap, in which the centrifugal acceleration already induces the sedimentation of the particles. At the same time, fresh feed mixes with returning particles that have already been separated in the disk gaps. Thereby, the sedimentation domain is assumed to be ideally back-mixed. The separated particles form the sediment in the solids space, whereby the shape and consolidation of the sediment are described with the help of a model for compression resistance. The product flow divides into the disk gaps.

Assuming that the product flow is evenly distributed, solely one disk gap is considered (domain II). Again, the individual compartments along the disk gap in which the sedimentation takes place were assumed to be ideally back-mixed. The movement of the separated particles on the underside of the disk back to the outer annular gap was calculated analytically. The separation of suspension and sediment is very different, so we divide the domain into two zones for sedimentation and sediment formation Fig. 2. In the sedimentation zone, the residence time behavior of the suspension in the apparatus is reproduced by a series connection of a defined number of compartments. In contrast, the sediment formation and its transport are determined in the sediment zone. The critical solids volume fraction ϕ_{gel} was used to differentiate between particles that have already been separated and those that have not. If the solids volume fraction ϕ is less than ϕ_{gel}, the mixed phase is present as a suspension. If $\phi > \phi_{gel}$ applies, the particles are separated and the mixed phase is present as a sediment.

Overall, the modeling methodology is based on the following assumptions:

1: The particles are small in relation to the apparatus.
2: The particles are homogeneously distributed within each control volume in the separation area (ideal back- mixing).
3: All particles have the same shape and density
4: The particles and the fluid are incompressible.
5: No mass transfer occurs between the components.

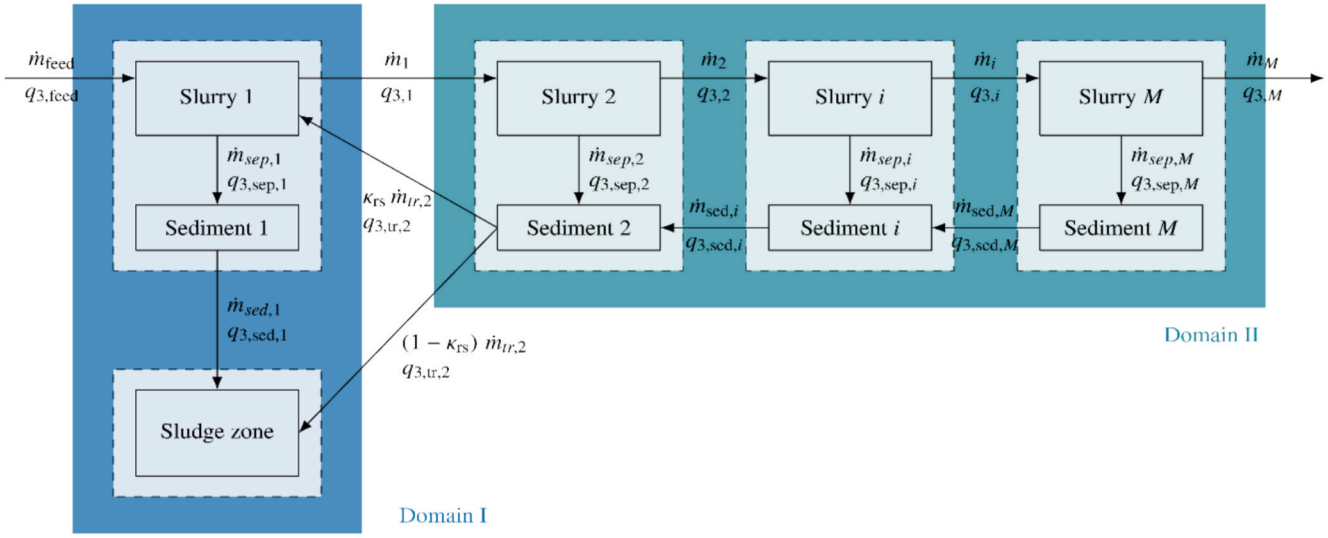

Fig. 2. Schematic representation of the compartment approach for the solids flux in the disk stack separator.

6: No agglomeration, growth or breakage processes occur during the separation process.
7: The local change in the particle size distribution is described by the residence time distribution.
8: The volume flow is distributed evenly across the disk gaps.
9: The welded-on spacers are neglected.

In contrast to resolved CFD simulations, the model does not consider flow effects such as vortices or turbulence, back-mixing effects or dead zones. Instead, it is assumed that the flow profile in the entire apparatus is a plug flow profile according to Gleiß et al. [39] and Sinn et al. [45]. Since no data are available on the flow through the outer annular gap and the sludge zone, both the outer annular gap and the sludge zone were modeled in this work with only one compartment each. Whether and to what extent particles already separated in the outer annular gap are mixed back into the suspension is also currently uncertain. The back-mixing itself can depend on the flow conditions, which in turn depend on the apparatus geometry, but also on the material properties.

2.1. Material functions

The sedimentation behavior of finely dispersed particles significantly influences the separation performance in centrifuges. A larger solids volume fraction increases the hydrodynamic interactions between particles and the liquid and results in slower sedimentation velocity. This material behavior may be described using the hindered settling function

$$h(\phi) = \frac{u_p}{u_{p,St}} \tag{1}$$

which relates the actual slowed or hindered settling velocity u_p to the Stokes settling velocity $u_{p,St}$ and depends on the solids volume fraction ϕ of the slurry. According to Stokes [48], the settling velocity of a single, spherical particle

$$u_{p,St} = \frac{(\rho_s - \rho_l)}{18\mu_l} x_p^2 \omega^2, \tag{2}$$

with the diameter x_p depends on the difference between the densities of the solid phase ρ_s and the liquid phase ρ_l, the liquid phase's viscosity μ_l and the acceleration. In centrifuges, the acceleration due to gravity g is replaced by the much stronger centrifugal acceleration, which is calculated from the radial position r and the angular velocity ω. A commonly used model for the hindered settling function originates from Michaels and Bolger [49] assuming that the settling hinderance is solely a function of the solids volume fraction ϕ:

$$h(\phi) = k_1 \left(1 - \frac{\phi}{\phi_{max}}\right)^{k_2} \tag{3}$$

Here, the parameter ϕ_{max} describes the maximum solids volume fraction, k_1 and k_2 are empirical parameters. The combination of equations Eq. (1), Eq. (2) and Eq. (3) gives the sinking velocity of particle

$$u_p = \frac{(\rho_s - \rho_l)}{18\mu_l} x_p^2 \omega^2 k_1 \left(1 - \frac{\phi}{\phi_{max}}\right)^{k_2} \tag{4}$$

In addition to the settling behavior of the particles, the sediment formation plays an important role in centrifuges. The characteristics of the sediment depend significantly on the properties of the disperse phase, such as particle size or particle shape, and on the interactions between the particles. The compressible behavior of the sediment may be described by the compression resistance $\sigma_e(\phi)$ as a function of the solids volume fraction. The literature offers a large number of models [50,51,52,53] to describe this material function. In this paper, the compression behavior is described using the power approach of Green et al. [52].

$$\sigma_e(\phi) = p_1 \left[\left(\frac{\phi}{\phi_{gel}} \right)^{p_2} - 1 \right] \tag{5}$$

Here, p_1 and p_2 are empirical parameters. In addition, the solids volume fraction is related to the gel point ϕ_{gel} which is an important material parameter. The gel point ϕ_{gel} is the critical solids volume fraction which marks the transition between slurry and sediment. For $\phi < \phi_{gel}$ the particles are not settled and slurry is present. For $\phi \geq \phi_{gel}$ the particles are separated and form a network, characterized by permanent particle–particle contacts and consequently sediment is present.

2.2. Control volumes and their discretization

The sedimentation zone mathematically summarizes the sedimentation behavior of the disperse phase in the separation apparatus. For this purpose, the sedimentation of the individual particle size classes is reevaluated in each compartment i. Thereby, the simulation of the particle transport in a control volume is based on a solids mass balance for each particle size class n

$$\frac{dm_{n,i}}{dt} = \dot{m}_{n,i-1}(t) - \dot{m}_{n,i}(t) - \dot{m}_{sep,n,i}(t) \tag{6}$$

The term on the left side describes the temporal change of the mass of the particle size class n in compartment i. The terms on the right side represent the sum of the mass fluxes involved: the flux of particles entering the considered control volume from the previous compartment $i-1$, the flux of particles leaving the compartment i and the flux of separated particles, which are consequently counted as sediment and no longer as slurry. A time-dependent separation efficiency $\eta_{sep,i}(t)$ is used as the separation criterion in each compartment:

$$\eta_{sep,i}(t) = \sum_{n=1}^{N} \frac{\dot{m}_{n,i}(t)}{\dot{m}_i(t)} T_{n,i}(t) \quad \text{with} \quad \dot{m}_i(t) = \sum_{n=1}^{N} \dot{m}_{n,i}(t) \tag{7}$$

The separation efficiency is defined as the ratio of the separated solids mass flow to the incoming solids mass flow [54]. Thereby, $T_{n,i}(t)$ describes the grade efficiency. Rearranging Eq. (7) and inserting it into Eq. (6) gives the following expression for the mass balance:

$$\frac{dm_{n,i}}{dt} = \dot{m}_{n,i-1}(t) \left[1 - \eta_{sep,i}(t) - \frac{\dot{m}_{n,i}(t)}{\dot{m}_{n,i-1}(t)} \right] \tag{8}$$

To determine the solids volume fraction ϕ_i, the mass balance can be converted to a volume balance assuming a constant solid density.

$$\frac{dV_i\phi_i}{dt} = \dot{V}_{i-1}(t)\phi_{i-1}(t) \left[1 - \eta_{sep,i}(t) - \frac{\dot{V}_i(t)\phi_i(t)}{\dot{V}_{i-1}(t)\phi_{i-1}(t)} \right] \tag{9}$$

For the control volume, through which the suspension enters the apparatus through the inlet of the centrifuge, the boundary conditions for the incoming volume flow $\dot{V}_{i-1} = \dot{V}_{in}$ and the solids volume fraction $\phi_{i-1} = \phi_{in}$ are specified. In Fig. 2, the sedimentation zone is labeled as *Slurry*. The indices i and $i-1$ indicate the mass flows transported into and out of the control volume. Analogous to the suspension zone (Eq. (6)), a mass balance can be formulated for the sediment zone.

$$\frac{dm_{sed,n,i}}{dt} = \dot{m}_{sep,n,i}(t) + \dot{m}_{sed,n,i}(t) - \dot{m}_{sed,n,i-1}(t) \tag{10}$$

The particles that are separated out of the suspension control volume enter the sediment control volume. At time $t = 0$ s, there is no sediment present yet. This means that the separated particles form the sediment. The centrifugal force causes the sediment in the disk gab (domain II) to slide along the bottom of the upper disk toward the solid space. At time $t > 0$ s, the particles that have been separated are added to the sediment that has already been separated and is located in the compartment. Since

the sediment fills a defined volume of the apparatus and thus influences the free flow cross-section as well as the separation distance, Eq. (10) is converted into a volume balance.

$$\frac{d\phi_{sed,i}V_{sed,i}}{dt} = \phi_{sep,n,i}(t)\dot{V}_{sep,n,i}(t) + \phi_{sed,n,i}(t)\dot{V}_{sed,n,i}(t) - \phi_{sed,n,i-1}(t)\dot{V}_{sep,n,i-1}(t) \tag{11}$$

The amount of solids that are separated is calculated from the separation efficiency.

$$\dot{V}_{sep,n,i}(t) = \phi_i(t)\dot{V}_i(t)\eta_{sep,i}(t) \tag{12}$$

2.3. Modeling of sedimentation and separation

The separation efficiency or grade efficiency is the last unknown variable for determining separation in the sedimentation zone (see Fig. 2: *Slurry*). According to Beiser [55] and Gleiß [40], the grade efficiency is based on an ideally mixed compartment, meaning that all particles are evenly distributed across the entire flow cross-section. In this case, the grade efficiency results from the volume V_{sep} in which the particles are separated in relation to the total available volume V_{tot}.

$$T_{n,i}(t) = \frac{V_{sep,i}(t)}{V_{slurry,i}(t)} = \frac{V_{tot,i} - V_{sed,i}(t) - V_{crit,i}(t)}{V_{tot,i} - V_{sed,i}(t)} \tag{13}$$

When particles settle and form sediment, they reduce the volume available for separation. At the start ($t = 0$ s), no sediment is present ($V_{sed,i} = 0$ m^3), thus the volume V_{slurry} which the slurry flows through is equal to the volume of the compartment meaning $V_{slurry,i} = V_{tot,i}$. After the start of the separation, the available volume $V_{slurry,i}$ depends on the time and the volume of the sediment $V_{sed,i}$. The total volume $V_{tot,i}$ of each control volume corresponds to that of a hollow cylinder according to the Pappus–Guldinus theorem.

$$V_{tot,i} = \pi h\left(R_{i-1}^2 - R_i^2\right) \tag{14}$$

The radii R_{i-1} and R_i denote the radial dimensions of the control volume. In domain I, h is the height of the entire disk stack h_{ds} and in domain II, h is the height of the disk gap h_{gap}. Fig. 3 schematically shows the modeling approaches used to determine the volume in which all particles are separated in order to calculate the grade efficiency (Eq. (13)). The separation volume depends on the critical radius (domain I) or the critical height (domain II).

Domain I

A balance of forces for each particle class links the two velocity components that contribute to the overall particle motion. On the one hand, the particles follow the main flow, on the other hand, they move outward in the radial direction due to the centrifugal force. For the main flow, it is assumed that the flow is uniform over the entire cross section with no back-mixing regions or velocity gradients in the radial direction. In domain I, the control volumes for sedimentation correspond to a tubular centrifuge. Assuming a plug flow, the residence time

$$t_{res,i} = \frac{\pi h_{ds}\left(R_{sed,i}^2(t) - R_i^2\right)}{\dot{V}_{feed,i}(t)} \tag{15}$$

can be calculated from the ratio of the respective control volumes to the volume flow $\dot{V}_{feed}$. Initially, there is no sediment $R_{sed} = R_{i-1}$. As soon as the deposition of particles begins, the growing sediment leads to a reduction of the cross-sectional area and thus to a decrease of the residence time in the control volume. At the same time, the growing sediment reduces the sedimentation distance, which affects the settling time. The settling time $t_{settling,i}$ is defined as the ratio of the settling velocity (Eq. (4)) and the available sedimentation length.

$$t_{settling,i} = \frac{18\mu_l}{(\rho_s - \rho_l)\omega^2 x_p^2} ln\left(\frac{R_{sed,i}(t)}{R_i}\right) \tag{16}$$

If a particle is deposited within the control volume, it satisfies the criterion that its residence time is greater than or equal to its settling time. Equating the residence time with the sedimentation time allows to derive a critical initial position of the particles $R_{crit,i}$, where they are just barely separated.

$$R_{crit,i}(t) = R_{sed,i}(t)\exp\left[-\frac{\pi h_{ds}\left(R_{sed,i}^2(t) - R_i^2\right)}{\dot{V}_{feed,i}(t)}\frac{(\rho_s - \rho_l)}{18\mu_l}\omega^2 x_p^2 h(\phi,t)\right] \tag{17}$$

Since the height of the disk pack can be reduced in Eq. (13), the grade efficiency for domain I can solely be calculated from the ratio of the radii.

$$T_{n,i}(t) = \frac{R_{sed,i}^2(t) - R_{crit,i}^2}{R_{sed,i}^2(t) - R_i^2} \tag{18}$$

Inserting $R_{crit,i}(t)$ (Eq. (17)) into Eq. (18) gives the mathematical correlation of the grade efficiency

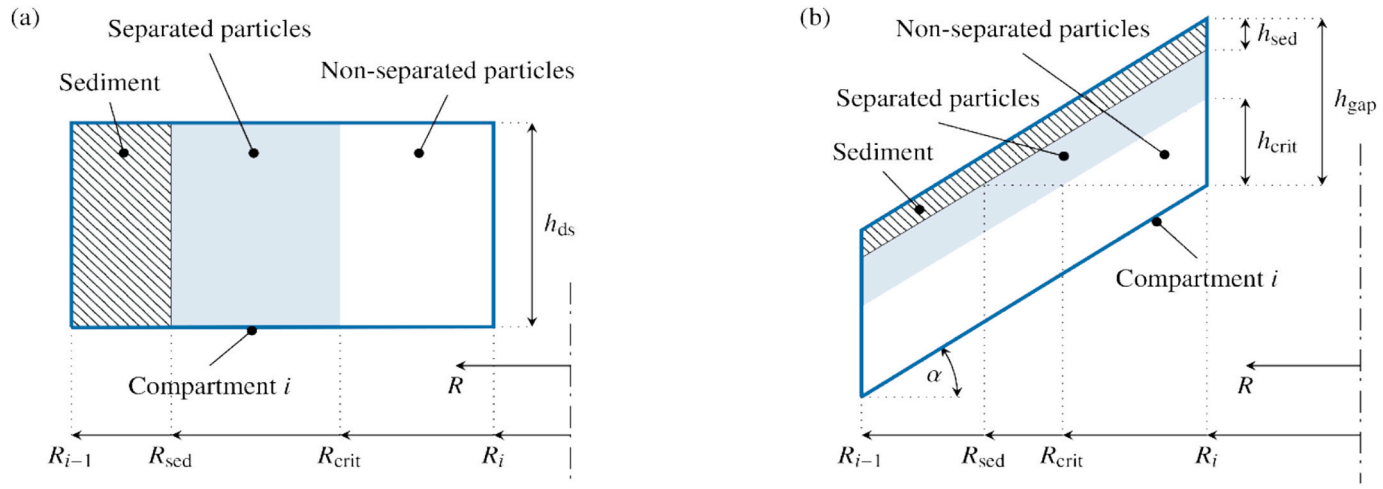

Fig. 3. Calculation of the critical length dimensions in the disk separator: (a) shows the approximation for the outer annular gap and for the sludge ports (domain I) and (b) shows a single gap (domain II) representing the entire disk stack. The region where all particles are separated is colored blue. (For interpretation of the references to colour in this figure legend, the reader is referred to the web version of this article.)

$$T_{n,i}(t) = \frac{R_{sed,i}^2(t)}{R_{sed,i}^2(t) - R_i^2}\left(1 - \exp\left[-\frac{\pi h_{ds}\left(R_{sed,i}^2(t) - R_i^2\right)}{\dot{V}_{feed,i}(t)}\frac{(\rho_s - \rho_l)}{18\mu_l}\omega^2 x_p^2 h(\phi,t)\right]^2\right) \quad (19)$$

as a function of the material properties, the simplified bowl geometry of the apparatus and the process conditions. The particles are considered separated when they reach the sludge port within the annular gap or the sediment surface.

Domain II

For domain II, assuming that the volume flow is evenly distributed across all disk gaps, one single disk gap is calculated as a representative for the whole disk stack. Again, the flow within the gaps is assumed to be plug flow. Therefore, the residence time $t_{res,i}$ does not only depend on the volume flow $\dot{V}_{feed,i}$, but also on the number of disk gaps n_{gap} :

$$t_{res,i} = \frac{\pi\left(h_{gap} - h_{sed,i}(t)\right)\left(R_{i-1}^2 - R_i^2\right)}{\frac{\dot{V}_{feed,i}}{n_{gap}}} \quad (20)$$

The control volumes in domain II has a conical shape. The most unfavorable starting point for the sedimentation of a particle is at the smallest radial position R_i. The sedimentation time $t_{settling,i}$ of a particle is defined as the time it takes for the particle to move radially from the worst starting position to the bottom of the overlying disk. Accumulated sediment reduces the sedimentation distance.

$$t_{settling,i} = \frac{18\mu_l}{(\rho_s - \rho_l)\omega^2 x_p^2} ln\left(\frac{R_{sed,i}(t)}{R_i}\right) \quad (21)$$

The radial position of the disk and the sediment can be determined from the angle α and the gap height h_{gap} and the sediment height $h_{sed,i}(t)$.

$$R_{sed,i}(t) = R_i + \frac{h_{gap} - h_{sed,i}(t)}{\tan\alpha} \quad (22)$$

Equating the residence time (Eq. (20)) and the settling time (Eq. (21)) gives the critical radial position $R_{crit,i}$.

$$R_{crit,i}(t) = R_i \exp\left[-\frac{\pi\left(h_{gap} - h_{sed,i}(t)\right)\left(R_{i-1}^2 - R_i^2\right)}{\frac{\dot{V}_{feed,i}}{n_{gap}}}\frac{(\rho_s - \rho_l)}{18\mu_l}\omega^2 x_p^2 h(\phi,t)\right] \quad (23)$$

which in turn results in a critical height $h_{crit,i}$.

$$h_{crit,i}(t) = \left(R_{crit,i}(t) - R_i\right)\tan\alpha \quad (24)$$

In this model, the sedimentation behavior of the particles assumes of very fine particles and slow flow. The hydrodynamic interactions between particles and the fluid are summarized as the sedimentation hindrance (Eq. (1)). Since the radii limiting the control volume are constant and thus can be reduced in Eq. (13), the grade efficiency in domain II can be calculated solely from the height ratios.

$$T_{n,i}(t) = \frac{h_{gap} - h_{sed,i}(t) - h_{crit,i}(t)}{h_{gap} - h_{sed,i}(t)} \quad (25)$$

Inserting Eq. (23) and Eq. (24) for $h_{crit,i}$ into Eq. (25) gives the mathematical correlation of the grade efficiency

$$T_{n,i}(t) = \frac{h_{gap} - h_{sed,i}(t) - R_i \cdot \tan\alpha\left(\exp\left[-\frac{\pi\left(h_{gap} - h_{sed,i}(t)\right)\left(R_{i-1}^2 - R_i^2\right)}{\frac{\dot{V}_{feed,i}}{n_{gap}}}\frac{(\rho_s - \rho_l)}{18\mu_l}\omega^2 x_p^2 h(\phi,t)\right] - 1\right)}{h_{gap} - h_{sed,i}(t)} \quad (26)$$

which contains all the necessary information for an efficient and comprehensive description of the separation behavior in the disk gap: material properties, geometry parameters of the disk stack and operating parameters. Within the disk gap, the particles of the inflowing volume flow $\dot{V}_{i-1}$ from the previous compartment settle and are considered separated when they reach the upper edge of the disk or the sediment surface.

2.4. Modeling of sediment formation

Finely dispersed suspensions tend to form compressible flowable sediments as the influence of interparticle interactions increases [50]. The porosity is a function of the compression resistance and decreases in the radial direction. Gleiß et. al. [39,40] have developed an algorithm that describes the consolidation behavior in solid bowl centrifuges. First, the mass of solids in the sediment $m_{p,sed,i}$ is determined. As a starting point, the solids volume fraction in the sediment is set to the gel point ϕ_{gel} for which the volume

$$V_{sed,i}(t) = \frac{m_{p,sed,i}(t)}{\rho_s \phi_{gel}} \quad (27)$$

and radial position of the sediment are determined. By rearranging Eq. (14), the radius of the sediment surface is

$$R_{sed,i}(t) = \sqrt{R_i^2 - \frac{V_{sed,i}(t)}{\pi h_{ds}}} \quad (28)$$

for domain I and

$$R_{sed,i}(t) = R_i - \frac{V_{sed,i}(t)}{\pi\left(R_{i-1}^2 - R_i^2\right)\tan\alpha} \quad (29)$$

for domain II by combining Eq. (24) also starting from the smallest radial position. In fact, this is only true for the topmost layer in a compressible sediment which is unstressed. Whereas the layers below in turn experience the pressure of the layers above. For this reason, the sediment is next divided into a defined number of M layers, where j is the counter, starting with $j = 1$ at the sediment surface.

$$V_{sed,i,j}(t) = \frac{V_{sed,i}(t)}{M} \quad (30)$$

The basis for modeling the sediment formation and its compaction is the differential equation according to Sambuichi [56]

$$\sigma_{e,j} = (\rho_s - \rho_l)\phi_{sed,i,j}\omega^2\left(R_j^2 - R_{j-1}^2\right) + \sigma_{e,j-1} \quad (31)$$

which describes the normal stress due to the centrifugal force acting on

each sediment layer in the radial direction. Thereby, no centrifugal pressure acts on the topmost layer $\sigma_{e,1} = 0$ Pa. Assuming the sediment is in equilibrium, the solids volume fraction in each layer is calculated using the material function for the compressive resistance (Eq. (5)). Now, the solids volume fraction in all layers of the sediment can be determined, allowing the radial position of the sediment to be calculated. Since the compressive resistance depends on the solids volume fraction, which is unknown in each layer, the consolidation state is determined iteratively starting from the gel point. The total sediment volume is the sum of the volumes of the compressed sediment layers.

$$V_{sed,i}(t) = \sum_{j=1}^{M} V_{sed,i,j}(t) \frac{\phi_{i,j}(t)}{\phi_{c,i,j}(t)} \tag{32}$$

The sediment volume of each layer is calculated by comparing the solids volume fraction $\phi_{i,j}$ before and $\phi_{c,i,j}$ after compression. The solids mass within the sediment does not change. Subsequently, the radial position of the sediment is determined again. The calculation will stop when the desired level of convergence is reached. The sediment formation results in a reduction of the flow cross section. As a result, the volume available for sedimentation decreases, causing the residence time of the particles to shorten. As the residence time decreases, less particles are separated because they settle more slowly than they remain in the compartment resulting the particle size distribution of the centrate shifts toward coarser particles. When the sediment exceeds a maximum radius or height, it is assumed that the residence time is so short that no further solids can settle in that zone.

2.5. Modeling of the sediment transport in the disk gap

For small time steps Δt, the modeling of the sediment transport in the disk gap is done analytically based on the inclined plane principle. In this case, the component of the weight force directed downward parallel to the inclined plane is known as the accelerating force F_a. In the centrifugal field, the weight force corresponds to the centrifugal force F_c.

$$F_a = F_c \cos\alpha \tag{33}$$

The accelerated force parallel to the disk gap depends on the disk angle α. The movement of the sediment along the underside of the upper disk is assumed to be uniformly accelerated in each compartment i, which means that the acceleration a_i is assumed to be constant. According to Newton's second law, the acceleration is proportional to the applied force F_a.

$$F_a = m_i a_i = m_i R_i \omega^2 \tag{34}$$

Again, the calculation of the acceleration acting in compartment i is based on the most unfavorable radial position R_i. Substituting Eq. (33) into Eq. (34) shows that the same acceleration a_i acts on all objects in an inclined plane, regardless of their mass m_i.

$$a_i = R_i \omega^2 \cos\alpha \tag{35}$$

The radial displacement $R_{d,i}$ can then be calculated as a function of the time interval Δt.

$$R_{d,i}(t) = R_i + R_i \frac{1}{2} \Delta t^2 \omega^2 \cos^2\alpha \tag{36}$$

It is assumed that the entire sediment is transported in the respective compartment. If the radial displacement is too large for the selected time step width, the separated solids are transported through several compartments towards the sludge zone.

3. Experimental procedure

The experiments include both material characterization and experiments with the disk separator to validate the developed model. The material characterization is performed on a laboratory scale. The model particle system used was polyvinyl acetate (PVAc). The continuous phase was deionized water. The material functions derived from the experiments form the basis for the integration of the real material behavior into the dynamic simulation model.

3.1. Material characterization

Important material functions are the particle size distribution, the hindrance settling function and the compression behavior. The particle size distribution was determined using the CPS24000 analytical disk centrifuge (CPS Instruments Inc., Prairieville, Louisiana, USA) which uses sedimentation of particles in liquids to determine particle size distribution. A density gradient is first established in the rotating process chamber using sugar solutions of different concentrations. At the outer edge of the disk, a laser shines through the transparent disk and hits the detector positioned behind it. The injected particles sediment according to their size. Particles of the same size form a band that moves outward and is simultaneously registered by the detector. From the time the particles take to reach the detector and the absorption of the light beam, the software calculates a particle size and a relative mass concentration for each fraction according to Stokes' law and Mie's theory of light scattering.

Experimentally, the hindered settling function was determined by measuring sedimentation velocities and varying the solids volume fraction. The analytical centrifuge LUMiSizer (LUM GmbH, Berlin, Germany) allows the determination of the settling velocity which are calculated from the evaluation of spatial and time resolved changes in the extinction profiles (STEP technology) [57]. The cuvettes containing the samples are placed on a rotating disk. During centrifugation, light shines through the cuvette. The sedimentation of the particles causes the suspension to become increasingly clear as the particles accumulate at the bottom of the cuvette. The change in transmitted light is recorded over time and converted into a sedimentation rate. To determine the hindered settling function, the experimentally determined settling velocities are then related to the Stokes' settling velocity, which is derived from the particle size distribution measured with the CPS analytical disk centrifuge.

To distinguish between suspension and sediment, it is important to determine the gel point. The gel point was determined through equilibrium settling tests [52,58] with the LUMiSizer. The solids volume fraction at the top of the sediment corresponds to the gel point. This is lower than the average solids volume fraction of the sediment, as the sediment is compressed by its own weight. The variation of ϕ or the filling level changed the maximum compression resistance at the base of the settled sediment and thus the mean solids volume fraction in the sediment. The extrapolation to $\phi = 0$ resulted in the gel point.

Another material function describes the consolidation of the sediment. The compression behavior of the sediment was investigated using a beaker centrifuge (Hermle ZK 630 refrigerated centrifuge, HERMLE Labortechnik GmbH, Wehingen, Germany) and a cutting device developed by Reinach [59]. For this purpose, the suspension was centrifuged until a state of equilibrium was reached with regard to sediment compression. The bottom of the centrifuge cutting insert is movable, allowing the sediment to be removed layer by layer and the respective solids volume fraction to be determined. The equilibrium state makes it possible to calculate the consolidation state in each sediment layer. In addition to the centrifugal force and the buoyancy force, the layers above act on the layer i, which simultaneously presses on the layers below. Since the cross-sectional area A of the sediment is constant, the respective pressures are summed up instead of the forces [59].

$$\sigma_{e,i} = \omega^2 \frac{\rho_s - \rho_l}{\rho_s A} \left(\sum_{j=1}^{i-1} r_j \Delta m_{p,j} + \frac{r_i \Delta m_{p,i}}{2} \right) \tag{37}$$

The variable r refers to the radial position starting from the axis of rotation of the beaker centrifuge, Δm_p is the solid mass of the layer i. The

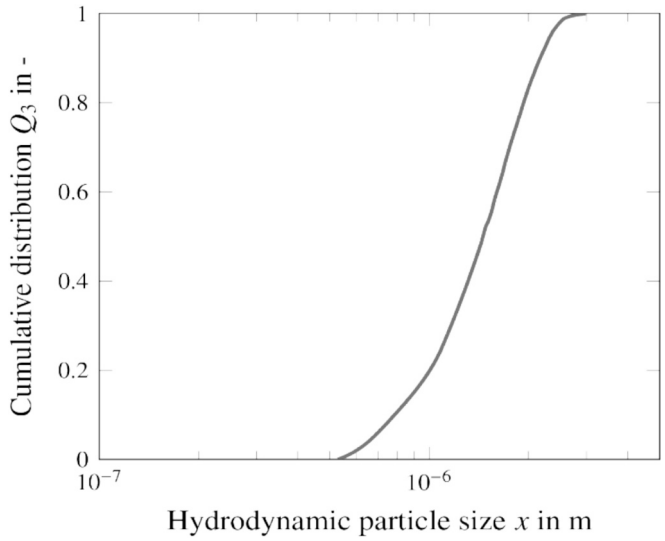

Fig. 4. Hydrodynamic particle size distribution pf PVA measured in the CPS disk centrifuge.

index j indicates the layers above the considered layer i. A detailed description for the experimental determination of the material functions is given by Zhai et al. [43].

PVAc is used to validate the dynamic model. This thermoplastic material is commonly found in wood glue. The PVAc utilized is from the company Henkel AG & Co. KGaA (Düsseldorf, Germany), whose product Ponal Classic was additionally diluted with deionized water for the validation experiments. Fig. 4 shows the particle size of the PVAc particles. The particle size distribution was determined using the CPS disk centrifuge. The PVAc has an average particle size of $x = 1.5$ µm.

3.2. Setup of the disk separator trial system

The simulation method is validated by comparing the simulation results with experiments on disk stack centrifuges at two different scales. Table 1 lists the geometric data of the two centrifuges. DSS-1 (machine type: SD1-06-107, GEA Westfalia Separator Group GmbH, Oelde, Germany) is the smaller centrifuge and has 57 disks, corresponding to an equivalent clarification area of 1150 m^2 according to the Σ-theory [14,15]. Whereas DSS-2 (machine type: CSC 8-06-477, GEA Westfalia Separator Group GmbH, Oelde, Germany) has 81 disks with a greater radius, resulting in an equivalent clarification area of 2180 m^2.

The suspension is placed in a feed vessel where an agitator ensures that the solid particles do not settle and are homogeneously distributed. Just before the separator, a valve allows sampling of the feed to measure the solids mass fraction and confirm the homogeneity of the suspension. The volume flow of the suspension, the rotational speed of the centrifuge and the emptying time of the sludge zone are adjustable. During the measurement process, all process parameters were set and then one of the operating parameters was varied. After each operating point, the separator was emptied several times through the sludge ports and rinsed with water to remove any sediment remaining in the apparatus. This ensures that previous tests do not influence the current series of measurements. To characterize the separation process, samples were taken after the centrifuge had reached a steady state. The volume fraction ϕ_p of solids in the sediment and centrate was determined.

$$\phi_p = \frac{w_s/\rho_s}{w_{s/\rho_s} + w_l/\rho_l} \tag{38}$$

For this purpose, the mass of the sample was measured in the wet and later in the dry state and the respective mass fractions w of the solids (s) and the liquid (l) were calculated.

Table 1
Geometry parameters of the disk separators used for model validation.

Parameter	Symbol	Unit	DSS-1	DSS-2
Disk angle	α	°	40	40
Gap height	h_{gap}	m	0.0007	0.0005
Number of gaps	n_{gap}	–	58	82
Minimum radius disk gap	r_{min}	m	0.024	0.034
Maximum radius disk gap	r_{max}	m	0.044	0.063
Radius sludge ports	r_{sp}	m	0.09	0.126

4. Results and discussion

Several physical processes take place in disk stack centrifuges that significantly influence the separation result. Laboratory-scale experiments form the basis of the simulation model to provide material functions to describe the sedimentation behavior and sediment formation. The model links the material functions with the residence time behavior and thus allows the dynamic simulation of the separation behavior in the disk stack centrifuge. The comparison of simulation results with experimental data on separation efficiency and mechanical dewatering serves to validate the developed mathematical model.

4.1. Experimentally determined material functions

PVAc is used to validate the dynamic model. It is based on material functions identified in laboratory experiments. Fig. 5 shows the determined material functions for the PVAc-water-suspension. The hindered settling function (left) was determined by measuring the settling velocities at different PVAc concentrations in the suspensions using the LUMiSizer.

The measured settling velocities were related to the Stokesian settling velocity derived from the particle size distribution obtained with the CPS disk centrifuge. The dashed line represents the model. At low solids volume fractions, the particles sediment freely according to their size. As the solids volume fraction increases, the particles progressively hinder each other, leading to a decrease in the sedimentation rate, i.e. the hindrance factor becomes smaller. The hindrance settling function can be described by Eq. (3), where the empirical parameters take the values $k_1 = 1$ and $k_2 = 30$. The maximum volume fraction of solids was assumed to be 0.74, corresponding to the maximum packing density for spherical particles. The sediment structure and compression behavior are defined by another material function. The consolidation function (right) describes the relationship between the solid effective stress and the solids volume fraction. The markers again indicate the experimental data, the dashed line represents the model. The compression behavior is described by the potency approach according to Green et al. [52] (Eq. (5)). The empirical parameters take the values $p_1 = 55{,}800$ Pa and $p_2 = 3.5$. The gel point is at $\phi_{gel} = 0.24$. Table 2 provides an overview of all material properties relevant for modeling.

4.2. Independency study

Compared to calculations with stationary models, dynamic simulation allows the description of important separation parameters such as level, solids volume fraction and separation efficiency as time-dependent variables. Key variables for the mathematical modeling are the time step size, the number of compartments and the number of sediment layers. The following results refer to the simulation of centrifuge DSS-2. All simulations were performed on a notebook with an Intel Core Ultra 7 155H processor (Intel Deutschland GmbH, Neubiberg, Germany).

Fig. 6 shows the dependence of the simulation result on the time step size (left) and the relation between the computation time and the time step size (right). The number of sediment layers was 30 and the disk gap

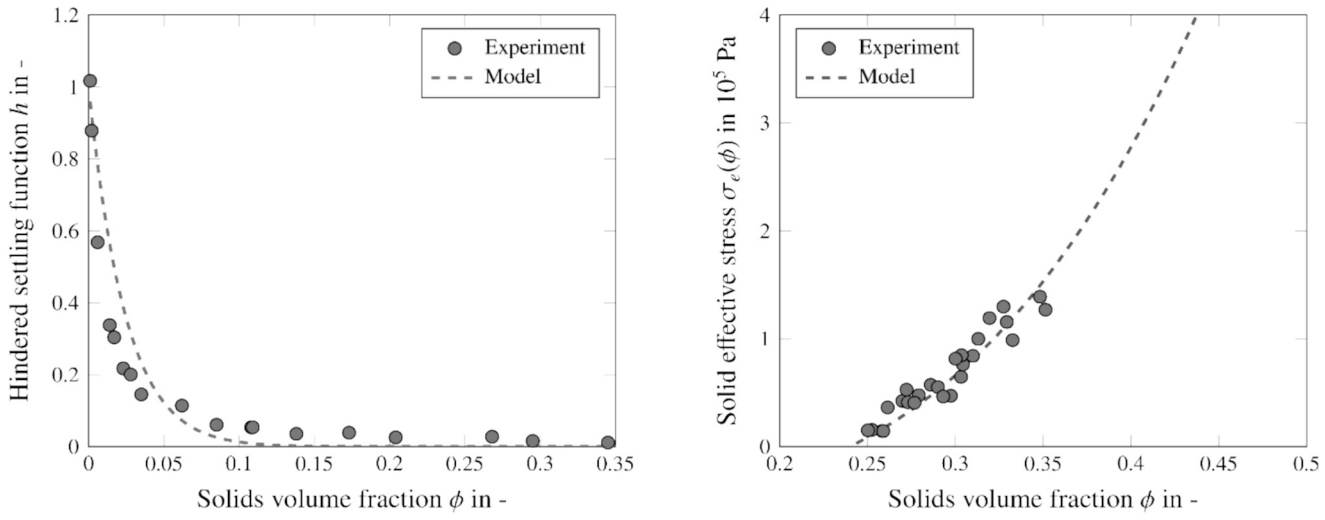

Fig. 5. Material functions of PVAc-water suspension: Influence of the solids volume fraction on the hindered settling velocity of a PVA-water suspension (left) and on the solids effective stress (right).

Table 2
Overview of the used material characteristics.

Parameter	Symbol	Unit	Diluted PVAc-suspension
Density difference solid and liquid	$\Delta\rho$	kg m^{-3}	170
Dynamic viscosity of liquid	μ_l	Pa s	0.004
Gel point	ϕ_{gel}	–	0.24
Maximum solids volume fraction	ϕ_{max}	–	0.74
Hindered settling parameter	k_1	–	1
Hindered settling parameter	k_2	–	30
Sediment compression parameter	p_1	Pa	55,800
Sediment compression parameter	p_2	–	3.5
Resuspending-factor	κ_{rs}	–	0

was resolved by 20 compartments. At the beginning, pure liquid flows through the separator. Starting from second 10, the feed concentration changed every minute.

The simulation results show that the solids volume fraction at the centrate outlet changes with time. At the same time, a clear shift can be seen for larger time steps. The reason for this is the assumption of a homogeneous distribution of the particles in each control volume, which causes an increase in back-mixing during the separation process. Furthermore, the start-up process at the beginning of the time-resolved simulation leads to a delayed discharge of the solids at the overflow. The initial flow through the apparatus has a significant influence on the residence time since it depends on the volume of the apparatus and the volume flow.

Looking at the computation time, it can be seen that time steps greater than or equal to 0.01 s are real-time capable, which means that they allow the process to be followed and tracked in real time.

In addition to the time step size, the number of compartments affects the accuracy of the simulation. Fig. 7 shows the solids volume fraction of the centrate plotted against time (left) and the dimensionless computational time as a function of the number of compartments (right). In this case, the time step is 0.02 s and the sediment are resolved by 30 layers. The simulation example corresponds to the upper scenario. Accordingly, pure fluid first flows through the separator before the solids volume fraction changes every minute. The simulation with one compartment

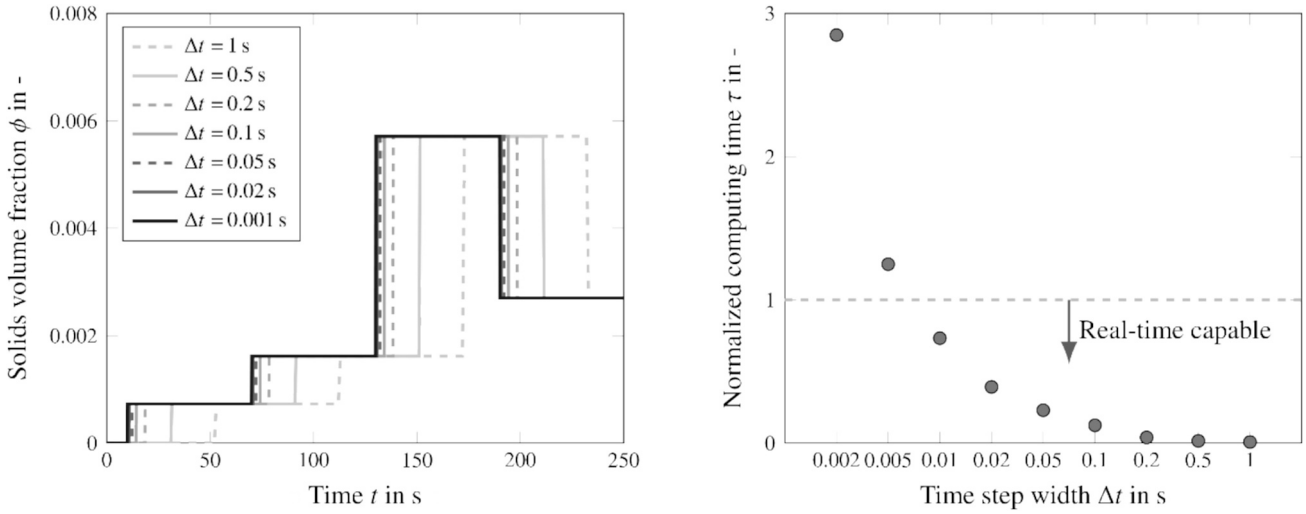

Fig. 6. Analysis of the temporal change of the solids volume fraction at the centrate outlet of a disk stack separator based on a sudden change in feed concentration from 0 to 0.5 % (t = 10 s), 1 % (t = 70 s), 2.5 % (t = 130 s) and 1.5 % (t = 190 s) (left) and the associated normalized calculation time as a function of the time step size (right). The disk gap was dissolved by 20 compartments, the sediment by 30 layers.

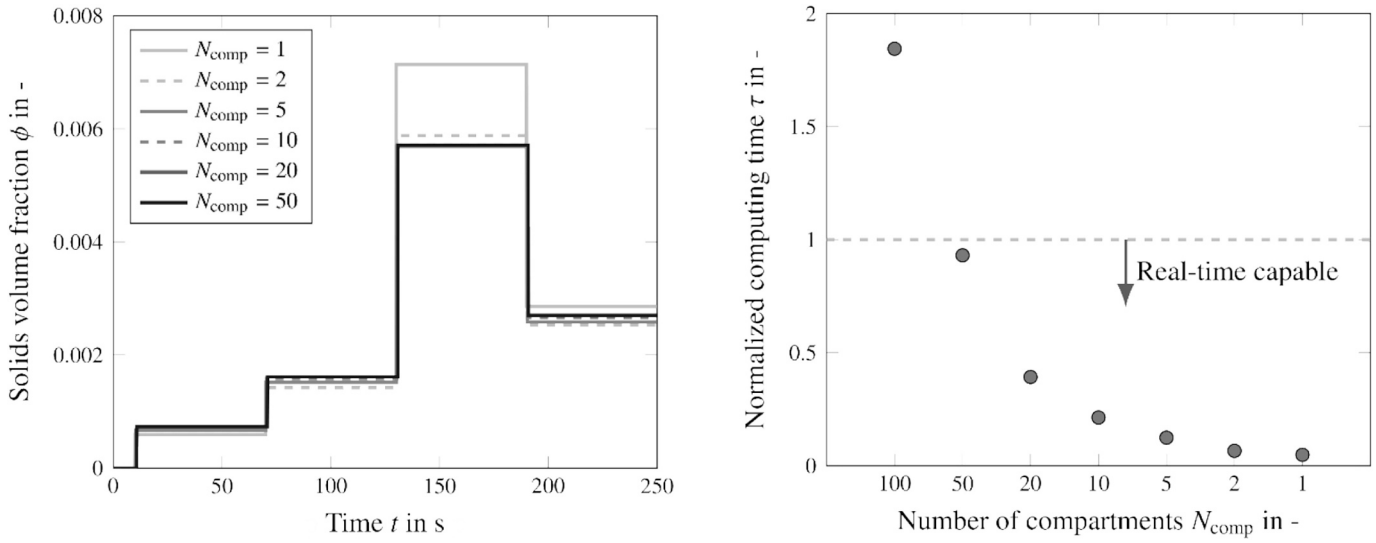

Fig. 7. Analysis of the time course of the solids volume fraction at the centrate outlet of a disk stack separator based on a sudden change in feed concentration from 0 to 0.5 % ($t = 10$ s), 1 % ($t = 70$ s), 2.5 % ($t = 130$ s) and 1.5 % ($t = 190$ s) (left) and the associated normalized calculation time as a function of the number of compartments (right). The time step width was $\Delta t = 0.02$ s and the sediment layer was dissolved by 30 layers.

results in a deviation of 14 % compared to the maximum number of 50 compartments shown here. Modeling with two compartments still shows a deviation of 10 %, whereas five compartments already show a significant reduction to just under 5 % deviation. In terms of computation time, the simulation time is still capable of real-time process monitoring for 50 compartments.

Besides the solids volume fraction of the centrate, the sediment properties determine the centrifuge's separation performance. Compressible sediments are characterized by a dependence of the solids volume fraction on the effective solids stress, resulting in an increase of the solids volume fraction in lower sediment layers. Fig. 8 shows the solids volume fraction in the sludge zone of the separator as a function of the number of sediment layers modeled (left) and the corresponding calculation time (right). In addition to the sediment that has already formed, the sludge also contains suspended solids. The simulation example also corresponds to the upper scenario where the solids volume fraction in the feed varies. It can be seen that the solids volume fraction in the sludge zone increases with time. With a higher solids content in the feed, more solids are fed into the centrifuge and more particles are separated, which means that the solids volume fraction in the sludge zone increases faster (greater slope).

The modeling with one layer and with two layers shows that the solids volume fraction in the sediment does not increase any further after 20 s and after 40 s, respectively. In these cases, the sludge zone is completely filled. The model issues a warning and no more solids are transported into the sludge zone compartment. Consequently, the solids are increasingly discharged with the centrate, which becomes turbid (not shown here). The sediment has little influence on the calculation time (right) compared to the time step width and the number of compartments. With a number of compartments of 30 and a time step of 0.02 s, the influence of the sediment on the computation time is only noticeable with a number of more than 20 sediment layers, while the simulation model is still real-time capable even with 50 sediment layers.

In summary, the accuracy improves as the time step size decreases

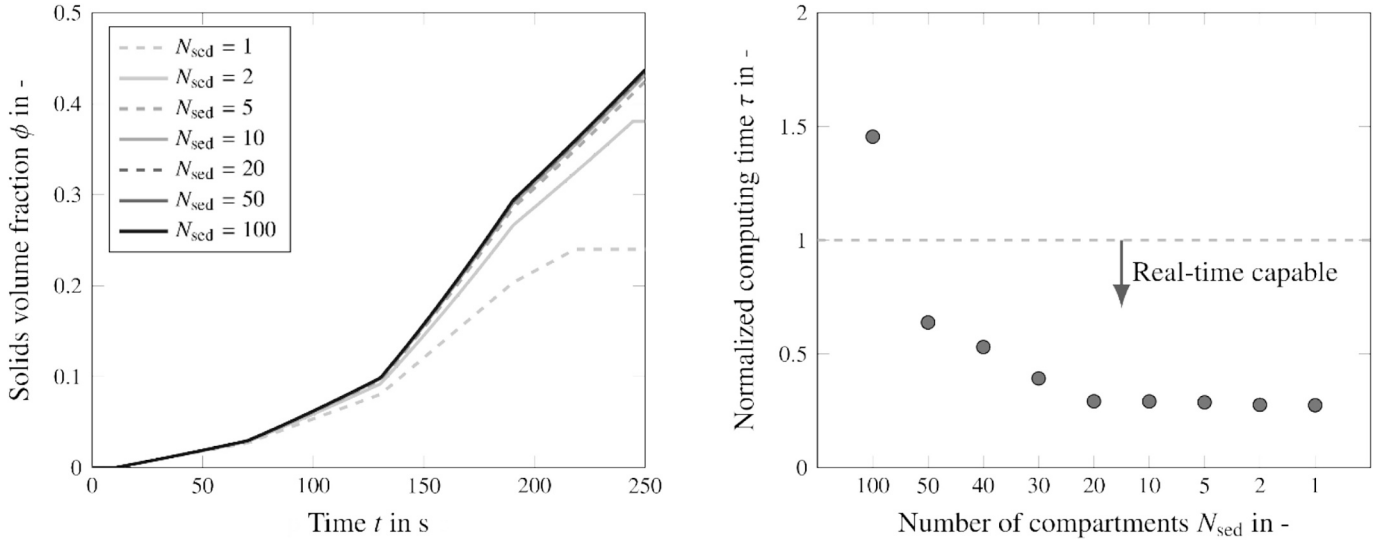

Fig. 8. Analysis of the time course of the solids volume fraction at the centrate outlet of a disk stack separator based on a sudden change in feed concentration from 0 to 0.5 % ($t = 10$ s), 1 % ($t = 70$ s), 2.5 % ($t = 130$ s) and 1.5 % ($t = 190$ s) (left) and the associated normalized calculation time as a function of number of sediment layers (right). The time step width was $\Delta t = 0.02$ s and the disk gap was dissolved by 20 compartments.

and the number of compartments and sediment layers increases. At the same time, the computational time grows with increasing accuracy. Based on the independence study, the simulations for the validation experiments were performed with a time step size of 0.02 s, 30 compartments and 20 sediment layers, which means that all results shown model the process in real time.

4.3. Validation of the separator model with experimental data

The validation includes a series of experiments focusing on the variation of significant process parameters. The aim is to investigate their influence on separation-relevant parameters such as separation efficiency or solids volume fraction in sediment and centrate. In addition, it will be verified that the simulations correctly reflect the respective dependencies and reproduce the experimental data. Fig. 9 illustrates the effect of the volume flow on the separation performance. The solids volume fraction of the centrate is shown on the left and the separation efficiency on the right. The separation efficiency is defined as the ratio of the separated solids mass flow to the incoming solids mass flow. If the residence time of the particles in the apparatus is high and the separation is complete, the separation efficiency is 1. As the residence time decreases, the separation efficiency tends to zero. In this validation experiment, the rotation speed is kept constant at 10,000 rpm which corresponds to 6,600 g related to the maximum radius. This series of tests was performed using the DSS-1 centrifuge. The marker indicates the experimental data, the dashed line the results of the simulation. Increasing the volume flow results in a shorter residence time of the suspension in the apparatus. This means that the particles have less time to settle. As a result, the solids volume fraction increases at higher flow rates and the separation efficiency decreases. Conversely, the residence time of the particles increases at lower flow rates, resulting in a decrease in the solids volume fraction of the centrate and the separation efficiency increases. Fig. 9 shows that the model provides good agreement with the experimental data.

The ability of the model to represent different scales is also important and needs to be investigated. For this reason, two separators of different sizes were used for validation. The following results were obtained using the DSS-2 centrifuge. Fig. 10 shows the solids volume fraction in the centrate (left) and the sediment (right) as a function of the volume flow. The different shades of gray indicate different rotational speeds. The markers represent the experimental results, the dashed lines refer to the simulation results. The sediment sample was collected by emptying the separator after five minutes. Increasing the volume flow shortens the residence time of the suspension in the centrifuge, and consequently reduces the time the particles have to settle. As a result, the solids volume fraction in the centrate rises as the volume flow increases. A higher volume flow also means that more particles enter the centrifuge, resulting in a faster filling of the apparatus. In turn, increasing the rotational speed causes a higher centrifugal force to act on the particles, separating more and smaller particles. Consequently, a higher rotational speed results in a reduction in the solids volume fraction of the centrate. At the same time, the formed sediment is compressed more. Both the experiment and the model reproduce these effects.

A direct comparison reveals that the compartment model underestimates the solids volume fraction in the centrate and overestimates it in the sediment, but reproduces the trend adequately. The discrepancy between the experimental results and the model outcomes is due to the accuracy of the material function (see Fig. 5). In this case, the solids content of the feed is very low. The model underestimates the hindrance to sedimentation within this range, meaning that particles sediment faster in the model than in reality. This can also be seen in Fig. 10, where the model assumes a higher solids volume fraction for the sediment (a higher settling velocity leads to a higher separation efficiency) and consequently a lower solids volume fraction in the centrate than the experimental data show.

The discrepancy between the experimental results and the model outcomes is due to the accuracy of the material function (see Fig. 5). In this case, the solids content of the feed is very low. The model underestimates the hindrance to sedimentation within this range, meaning that particles sediment faster in the model than in reality. This can also be seen in Fig. 10, where the model assumes a higher solids volume fraction for the sediment (a higher settling velocity leads to a higher separation efficiency) and consequently a lower solids volume fraction in the centrate than the experimental data show.

The comparison between simulated and experimental particle size distributions is shown in Fig. 11. Again, simulation and experiment show the same trend. As the volume flow increases (left), the residence time of the particles in the apparatus decreases. At lower flow rates and consequently higher residence times, the particles have more time to sediment and consequently even smaller particles are separated. Consequently, the particle size distribution of the particles in the centrate shifts to the left as the flow rate decreases. Another operating parameter is the rotational speed of the centrifuge. Increasing the speed results in greater centrifugal force, which separates more and simultaneously smaller particles. The particles removed with the centrate therefore become smaller, resulting in a shift of the particle size

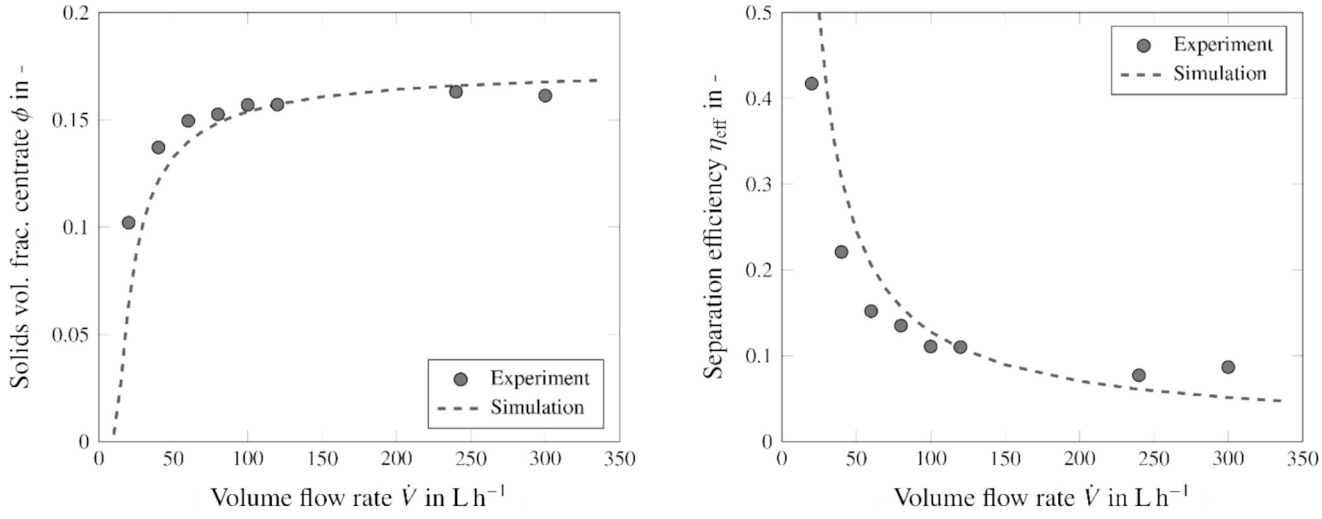

Fig. 9. Influence of the volume flow rate on the clarification performance as measured by DSS-1 at 6,600 g: solids volume fraction of the centrate (left) and separation efficiency (right).

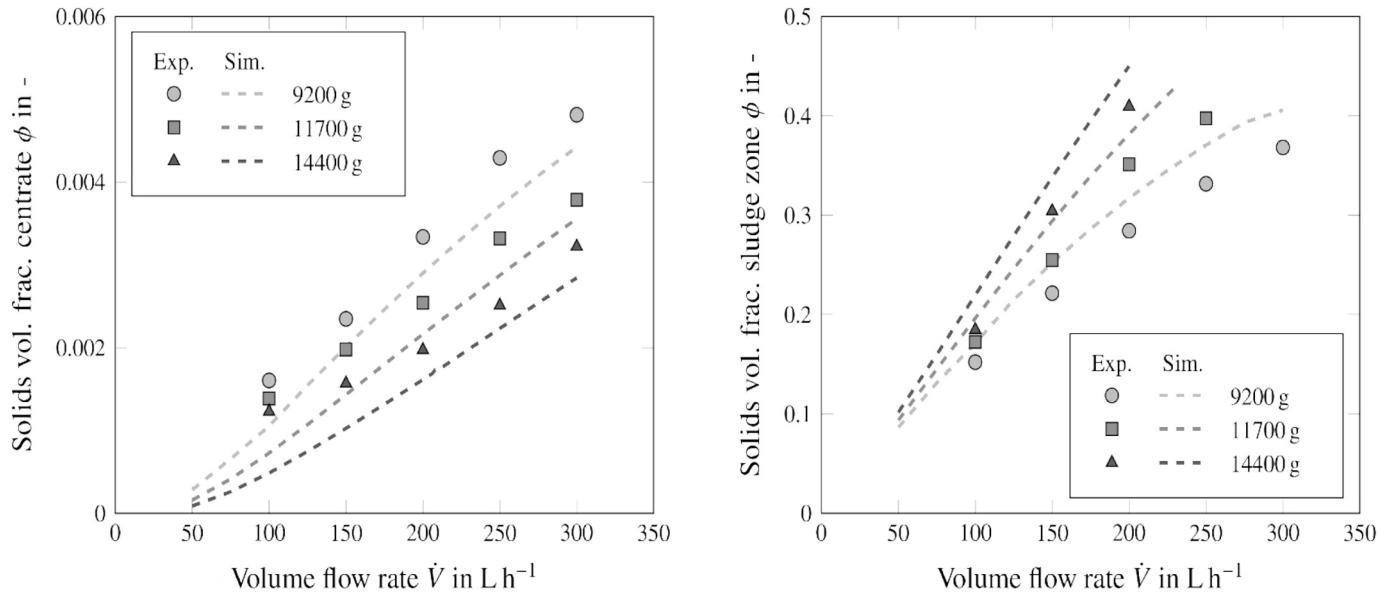

Fig. 10. Influence of the volume flow rate and the g-Force on the clarification performance as measured by DSS-2: solids volume fraction of the centrate (left) and solids volume fraction of the sediment (right) when the separator is emptied every five minutes.

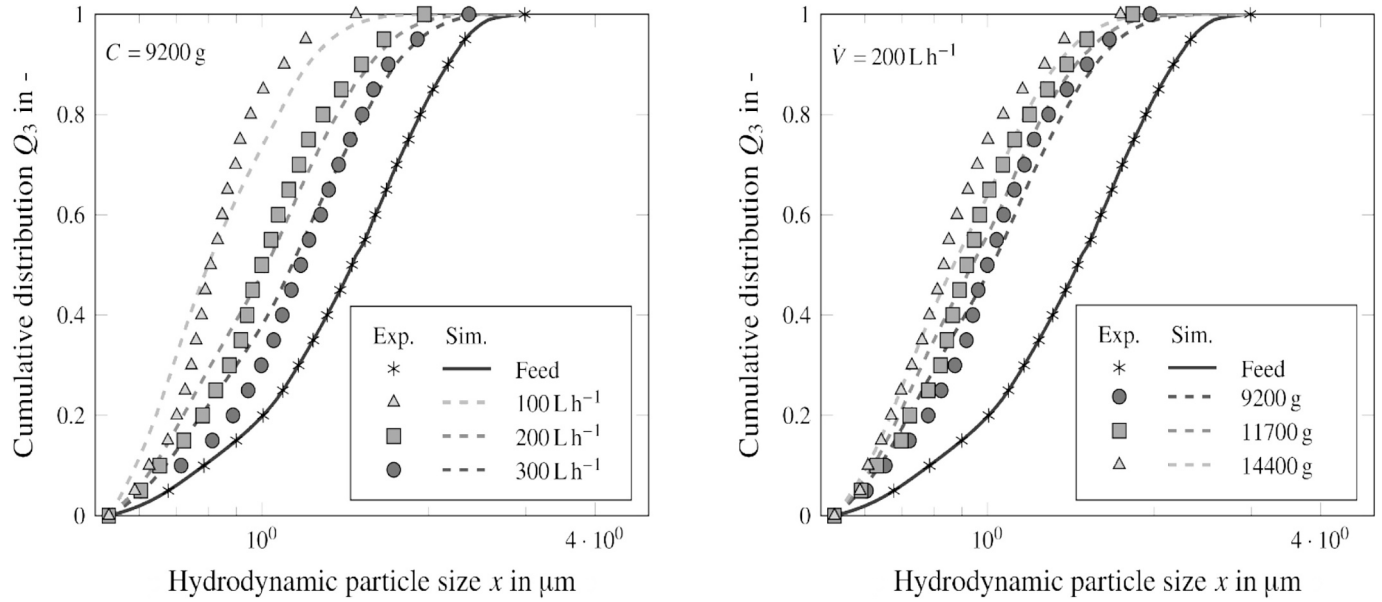

Fig. 11. Particle size distribution of the centrate at steady state for the dynamic simulation and the experiment varying the volume flow rate (right) and the rotational speed (left). The experiments were carried out using the DSS-2 separator.

distribution to the left. Both experiments and simulations show this behavior.

The differences between the experiment and the model may be due to uncertainties in the material function. The material function for sedimentation describes the hindrance during sedimentation, regardless of the particle size distribution. It is quite conceivable that different particle size classes are hindered or favored to varying degrees during sedimentation due to interaction with other particles.

Another aspect of interest is whether the model is able to reproduce the dynamic behavior of the process. Fig. 12 shows the filling process of the DSS-2 centrifuge. The solids volume fraction of the sludge zone is shown on the left, and the solids volume fraction of the centrate is shown on the right.

The test series consisted of several discharges of the separator. The separator was manually emptied several times before each measuring point. After a waiting period of five minutes, the separator was emptied again to ensure that it was filled and that all measurement points were collected under the same conditions. The entire slurry from the sludge zone was collected. A centrate sample was also taken immediately before each discharge. Before taking the next sample, the separator was manually emptied again and the cycle started anew. The interval between sampling points was two minutes. The volume flow was 85 L h^{-1} and the rotational speed was 8,100 rpm which corresponds to 9,200 g. During the first few minutes, the solids volume fraction in the sludge zone increases. In contrast, the solids volume fraction of the centrate remains constant. After about 12 min, the sludge zone is completely filled. The compartment representing the volume of the sludge zone cannot hold any more solids. The remaining part of the centrifuge fills up and the centrate becomes increasingly turbid. The solids volume fraction in the centrate continues to rise until it finally equals the feed

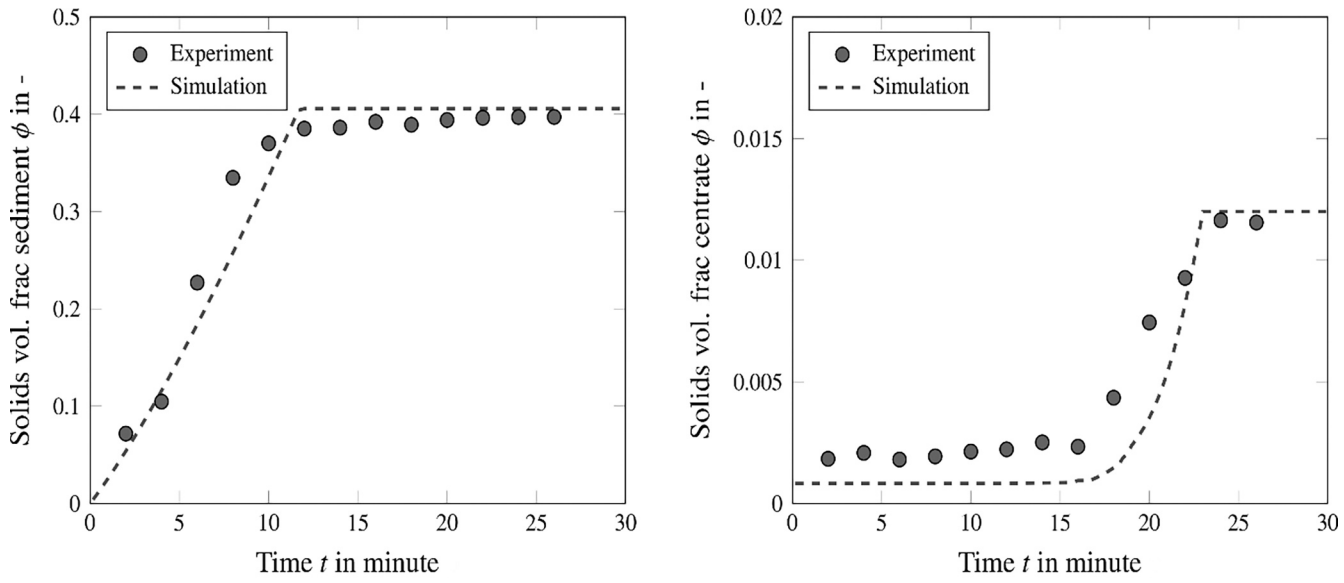

Fig. 12. Filling process of the separator DSS-2: Solids volume fraction of the sediment (left) and the centrate (right) at a volumetric flow rate of 85 L h^{-1} and a rotational speed of 9,200 g.

concentration after about 23 min. The simulation results are in good agreement with the experimental data. In particular, the filling of the sludge zone is well reproduced. However, the simulation underestimates the solids volume fraction of the centrate. In addition, the centrate turbidity starts slightly earlier in the experiment and is less steep than calculated by the simulation. Overall, the model provides a robust approximation of the dynamic behavior of the centrifuge filling process.

4.4. *Influence of geometric parameters*

The model also allows geometric parameters to be varied and their influence on separation efficiency to be studied. Fig. 13 shows the separation efficiency as a function of the number of disks (left) and the disk angle (right) for the separator DSS-1. Volume flow and g-force are constant with 200 L h^{-1} and 11,700 g in both examples. It can be clearly seen how increasing the available clarification area by raising the number of plates improves the separation performance. An increase in the number of disk gaps leads to a longer residence time of the suspension in the apparatus, so that the particles have more time to sediment. In reality, however, the number of disks depends on the height of the disk insert to be accommodated according to the respective machine dynamics, whereby the maximum number of disks results from the required disk thickness and the disk gap height [60]. The effect of the disk angle is shown on the right-hand side. An increase in the disk angle leads to a shortening of the sedimentation distance and therefore to an increase in the number of particles separated and thus to an increase in the separation efficiency. In practice, the disk angle is determined by the repose angle of the sediment to ensure reliable sliding on the underside of the disk [60]. Overall, the simulation model may help to identify the most suitable apparatus for the separation task.

5. Conclusion and outlook

This study presents a modeling approach for the real-time simulation of disk separators. The predictive model is based on machine and material functions, which allows dynamic simulation for changing operating parameters and feed material properties. As in the work of Gleiss and Menesklou [39–42], the separator is described by a defined number

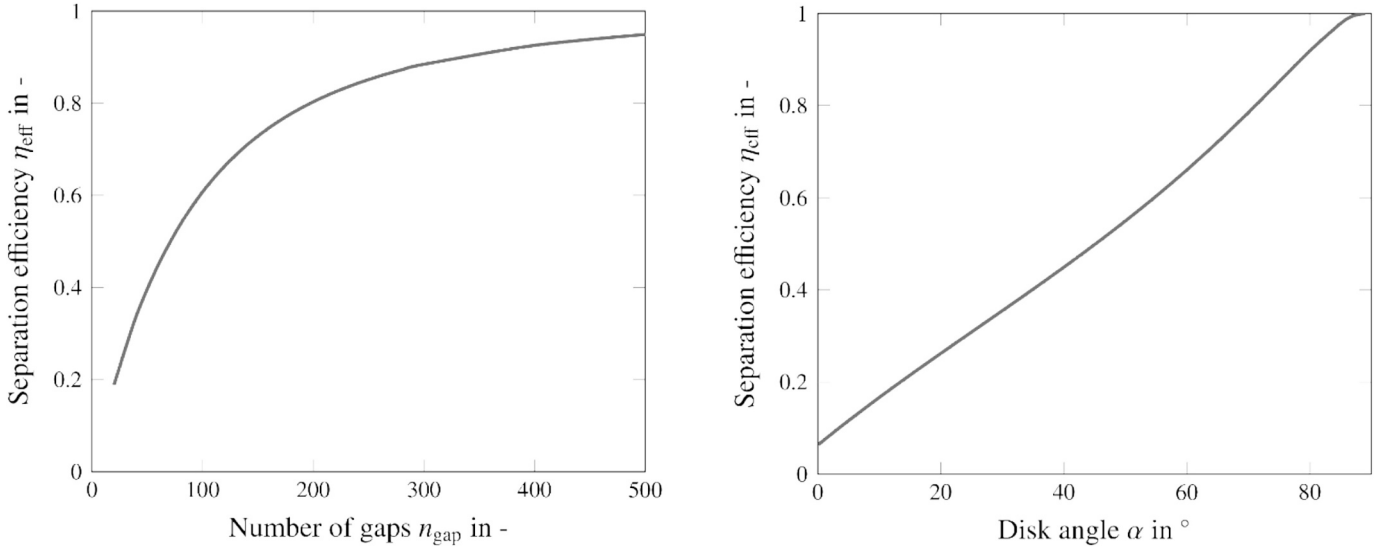

Fig. 13. Varying the number of disks (left) and disk angle (right) at constant volume flow rate (200 L h^{-1}) and rotational speed (9000 rpm).

of compartments in which balance equations for either sedimentation or sediment formation are solved. The resulting dynamic model of the disk separator simulates the separation process in real time. Validation experiments with two different separators were successfully reproduced by the model.

The transfer to other solid liquid separation devices such as filter apparatuses is conceivable. Depending on the application, the material function for sedimentation would possibly be replaced by one for filtration resistance through filter medium and cake. However, the existing models for the centrifuges can also be further refined: At present, the settling velocity depends solely on the solids volume fraction. The material parameters of the hindrance settling function are the same for all particle size classes. Baust et al. [61] have proposed a model that also considers the particle size itself as a further influencing parameter. However, the model does not take into account agglomeration or particle fragmentation. Furthermore, the gliding of separated particles or the sediment along the underside of the disk represents further potential. In this work, an analytical equation was implemented and the roughness of the plate and the repose angle of the sediment were neglected. By implementing a suitable gliding model and improving existing models, the accuracy of the model may be further improved.

In summary, an extension or addition of material functions enables an improvement in accuracy. Furthermore, the dynamic process model is a powerful and valid simulation method that can be used both as a stand-alone simulation tool for modeling the separation performance, for optimization, for model-predictive control and as part of an apparatus in an entire process chain.

6 Author statement

On behave of all authors, I confirmed that the manuscript is original and not be published in elsewhere.

CRediT authorship contribution statement

Helene Katharina Baust: Writing – review & editing, Writing – original draft, Software, Project administration, Methodology, Data curation. **Zihim Lam:** Methodology, Data curation, Conceptualization. **Michael Hay:** Writing – review & editing, Data curation, Conceptualization. **Hermann Nirschl:** Writing – review & editing, Supervision, Funding acquisition. **Marco Gleiß:** Writing – review & editing, Supervision, Project administration, Funding acquisition, Conceptualization.

Funding

This research was funded by the German Federal Ministry for Economic Affairs and Climate Action (Grant number: 03EN2062F).

Declaration of competing interest

The authors declare that they have no known competing financial interests or personal relationships that could have appeared to influence the work reported in this paper.

Acknowledgements

The authors would like to thank all students and colleagues who contributed to the successful completion of this work. They would also like to thank GEA Westfalia Separator Group GmbH for providing the disk stack separator. Furthermore, they acknowledge the support of the KIT Publication Fund of the Karlsruhe Institute of Technology (KIT).

Data availability

Data will be made available on request.

References

[1] K. Wintermantel, Process and product engineering achievements, present and future challenges, Chem. Eng. Res. Des. 77 (3) (1999) 175–188.
[2] R. Kempken, A. Preissmann, W. Berthold, Assessment of a disk stack centrifuge for use in mammalian cell separation, Biotechnol. Bioeng. 46 (2) (1995) 132–138.
[3] R.J. Wakeman, Separation technologies for sludge dewatering, J. Hazard. Mater. 144 (3) (2007) 614–619.
[4] H. Anlauf, Recent developments in centrifuge technology, Sep. Purif. Technol. 58 (2) (2007) 242–246.
[5] P.H. Chlup, D. Bernard, G.G. Stewart, Disk stack centrifuge operating parameters and their impact on yeast physiology, J. Inst. Brew. 114 (1) (2008) 45–61.
[6] V. Betalovic, Centrifugal separator, the new technical solution, application in mineral processing, Int. J. Miner. Process. 100 (3–4) (2011) 86–95.
[7] S.O. Majekodunmi, A review on centrifugation in the pharmaceutical industry, Am. J. Biomed. Eng. 5 (2) (2015) 67–78.
[8] G. Costagli, The use of disc stack centrifuge in the virgin olive oil industry, J. Agric. Eng. 49 (2) (2018) 70–80.
[9] T. Merkel, O. Blättler, S. Königsson, Flocculant screening method at lab scale for application in disc stack centrifuges with hermetic design, Chem. Eng. Technol. 41 (12) (2018) 2312–2322.
[10] W.A. Dryden, L.M. Larsen, D.W. Britt, M.T. Smith, Technical and economic considerations of cell culture harvest and clarification Technologies, Biochem. Eng. J. 167 (2021) 107892.
[11] H. Agarwal, C. Thwin, B.T. Kumaar, Single-use centrifugal separator enables intensification of the clarification process in biomanufacturing of recombinant proteins, J. Chem. Technol. Biotechnol. 98 (5) (2023) 1321–1332.
[12] H. Motta, N. dos Passos, M. Ambye-Jensen, Fractionation of proteins from alfalfa juice at demonstration scale: effects of temperature and centrifugation strategies on removal of green protein and recovery of the soluble white protein fraction, Sep. Purif. Technol. 330 (C) (2024) 125461.
[13] A. Brunner, Über das Reinigen von Schweröl mittels der Zentrifuge. Ph.D. Thesis, Eidgenössische Technische Hochschule Zürich, Switzerland 1956.
[14] C.M. Ambler, The theory of scaling up laboratory data for the sedimentation type centrifuge, J. Biochem. Microbiol. Technol. Eng. 1 (2) (1959) 185–205.
[15] C.M. Ambler, The fundamentals of separation, including Sharples Sigma-value for predicting equipment performance, Ind. Eng. Chem. 53 (6) (1961) 430–433.
[16] R. Wakeman, S. Tarleton, Solid/Liquid Separation: Scale-up of Industrial Equipment, 1st ed., Elsevier Advanced Technology, Oxford, UK, 2005.
[17] E.M. Goldin, Flow stability between separator plates, Mekhanika Zhidkosti i Gaza 1 (2) (1966) 152–155.
[18] K.-H. Brunner, Theoretische und experimentelle Untersuchung der Feststoffabscheidung in Tellerseparatoren. Ph.D. Thesis, Universität Erlangen-Nürnberg, Germany, 1979.
[19] K. Mannweiler, The recovery of biological particles in high-speed continuous centrifuges with special reference to feed-zone break-up effects. Ph.D. Thesis, University of London, UK, 1989.
[20] J. König, J. Ueding, U. Janoske, Analytical model to characterize the efficiency of disk stack separators, Chem. Ing. Tech. 92 (2020) 701–710.
[21] J. König, N. Janssen, U. Janoske, Visualization of the deposition mechanisms in disk stack centrifuges with an acrylic glass bowl top and high-speed image processing, Sep. Sci. Technol. 56 (3) (2021) 640–652.
[22] S. Schütz, M. Piesche, G. Gorbach, M. Schilling, C. Seyfert, P. Kopf, T. Deuschle, N. Sautter, E. Popp, T. Warth, CFD in der mechanischen Trenntechnik, Chem. Ing. Tech. 79 (11) (2007) 1777–1796.
[23] U. Janoske, M. Piesche, Numerical simulation of the fluid flow and the separation behavior in a single gap of a disk stack centrifuge, Chem. Eng. Technol. 22 (3) (1999) 187–260.
[24] U. Janoske, M. Piesche, Hydrodynamic investigations on the separation behavior of suspensions in a gap of a disk stack centrifuge with caulks, Chem. Eng. Technol. 23 (10) (2000) 829–921.
[25] M. Breitling, U. Janoske, M. Piesche, Numerische Simulationen transienter und turbulenter Strömungen zum Abscheideverhalten in Tellerseparatoren, Chem. Ing. Tech. 75 (3) (2003) 184–188 (In German).
[26] A. Zink, M. Piesche, P. Trautmann, M. Durst, Numerical and Experimental Investigations of a disk Stack Centrifuge Used as an Oil Mist Separator for Automotive Applications. SAE World Congress 2004, Detroit **2004**, Paper 2004-01-0638.
[27] E.D.L. Böndel, Fest-Flüssig-Trennung in Tellerseparatoren. Ph.D. Thesis, Universität Stuttgart, Germany, 2011. (In German).
[28] L.K. Shekhawat, J. Sarkar, R. Gupta, S. Hadpe, A.S. Rahore, Application of CFD in Bioprocessing: separation of mammalian cells using disk stack centrifuge during production of biotherapeutics, J. Biotechnol. 267 (2018) 1–11.
[29] P. Esmaeilnejad-Ahranjani, M. Hajimoradi, Optimization of industrial-scale centrifugal separation of biological products: comparing the performance of tubular and disk stack centrifuges, Biochem. Eng. J. 178 (2022) 108281.
[30] M. Dosta, J.D. Litster, S. Heinrich, Flowsheet simulation of solids processes: current status and future trends, Adv. Powder Technol. 31 (3) (2020) 947–953.
[31] J. Werther, S. Heinrich, M. Dosta, E.-U. Hartge, The ultimate goal of modeling—Simulation of system and plant performance, Particuology 9 (4) (2011) 320–329.
[32] V. Velasco-Mejıa, V. Vallejo-Becerra, A.U. Chavez-Ramirez, J. Torres-Gonzalez, Y. Reyes-Vidal, F. Castaneda-Zaldivar, Modeling and optimization of a pharmaceutical crystallization process by using neural networks and genetic algorithms, Powder Technol. 292 (2016) 122–128.

[33] P. Kazemi, M.H. Khalid, J. Szlek, A. Mirtic, G.K. Reynolds, R. Jachowicz, A. Mendyk, Computational intelligence modeling of granule size distribution for oscillating milling, Powder Technol. 301 (2016) 1252–1258.
[34] V.A. Rodriguez, L. Ribas, A. Kwade, L.M. Tavares, Mechanistic modeling and simulation of a wet planetary ball mill, Powder Technol. 429 (2023) 118901.
[35] F. Punt, S. doose, A.-C. Böttcher, S. Breitung-Faes, A. Kwade, Modeling and flow sheet simulation of selected mechanical recycling processes for Li-ion batteries, Chem. Ing. Tech. 95 (12) (2023) 59–67.
[36] M. Moreno-Benito, K.T. Lee, D. Kaydanov, H.M. Verrier, D. Blackwood, P. Doshi, Digital twin of a continuous direct compression line for drug product and process design using a hybrid flowsheet modelling approach, Int. J. Pharm. 628 (2022) 122336.
[37] M. Buchholz, J. Haus, L. Blesinger, C. Riemann, S. Pietsch, F.K. Jäger, S. Heinrich, Process design of a multistage drying process via flowsheet simulation, Chem. Ing. Tech. 93 (8) (2021) 1287–1294.
[38] H. Rehage, M. Semmel, M. Kind, A dynamic model for process flowsheet simulation of semi-batch precipitation of sparingly soluble salts, Comput. Chem. Eng. 137 (2020) 106818.
[39] M. Gleiß, H. Nirschl, Modeling separation processes in decanter centrifuges by considering the sediment build-up, Chem. Eng. Technol. 38 (10) (2015) 1873–1882.
[40] M. Gleiß, S. Hammerich, M. Kespe, H. Nirschl, Development of a dynamic process model for the mechanical fluid separation in decanter centrifuges, Chem. Eng. Technol. 41 (1) (2018) 19–26.
[41] P. Menesklou, H. Nirschl, M. Gleiss, Dewatering of finely dispersed calcium carbonate-water slurries in decanter centrifuges: about modelling of a dynamic simulation tool, Sep. Purif. Technol. 251 (2020) 117287.
[42] P. Menesklou, T. Sinn, H. Nirschl, M. Gleiss, Scale-up of decanter centrifuges for the particle separation and mechanical dewatering in the minerals processing industry by means of a numerical process model, Minerals 11 (2021) 229.
[43] O. Zhai, H. Baust, M. Gleiß, H. Nirschl, Model-based scale up of solid bowl centrifuges using experimentally determined material functions, Chem. Ing. Tech. 95 (2023) 189–198.
[44] M. Winkler, F. Rhein, H. Nirschl, M. Gleiss, Real-time modeling of volume and form dependent nanoparticle fractionation in tubular centrifuges, Nanomaterials 12 (2022) 3161.
[45] T. Sinn, P. Menesklou, H. Nirschl, M. Gleiss, Further developments of a dynamic real-time model of a tubular centrifuge fed with multi-component dispersions for application in fractionation for Direct Recycling of lithium-ion batteries, Chem. Eng. Sci. 277 (2023) 118858.
[46] V. Skorych, M. Buchholz, M. Dosta, H.K. Baust, M. Gleiß, J. Haus, D. Weis, S. Hammerich, G. Kiedorf, N. Asprion, H. Nirschl, F. Kleine Jäger, S. Heinrich, Use of multiscale data-driven surrogate models for flowsheet simulation of an industrial zeolite production process, Processes 10 (2022) 2140.
[47] N. Metta, M. Ghijs, E. Schäfer, A. Kumar, P. Cappuyns, I.V. Assche, R. Singh, R. Ramachandran, T. De Beer, M. Ierapetritou, I. Nopens, Dynamic flowsheet model development and sensitivity analysis of a continuous pharmaceutical tablet manufacturing process using the wet granulation route, Processes 7 (4) (2019) 234.
[48] G.G. Stokes, On the effect of internal friction of fluids on the motion of pendulums, Trans. Camb. Philos. Soc. 9 (1851) 8–106.
[49] A.S. Michaels, J.C. Bolger, Settling rates and sediment volumes of flocculated Kaolin suspensions, Ind. Eng. Chem. Fundam. 1 (1961) 24–33.
[50] R. Buscall, L.R. White, The consolidation of concentrated suspensions. Part 1. The theory of sedimentation, J. Chem. Soc., Faraday Trans. 1 83 (3) (1987) 873.
[51] K.A. Landman, L.R. White, M. Eberl, Pressure filtration of flocculated suspensions, AIChE J. 41 (7) (1995) 1687–1700.
[52] M.D. Green, M. Eberl, K.A. Landman, Compressive yield stress of flocculated suspensions: determination via experiment, AIChE J. 42 (8) (1996) 2308–2318.
[53] F.M. Tiller, J.H. Kwon, Role of porosity in filtration: XIII. Behavior of highly compactible cakes, AIChE J. 44 (10) (1998) 2159–2167.
[54] F. Löffler, J. Raasch, Grundlagen der mechanischen Verfahrenstechnik, Vieweg+ Teubner Verlag, Braunschweig, 1992.
[55] M. Beiser, Sedimentation submikroner Partikel in Abängigkeit physikalisch-chemicher Einflüsse und ihr Separationsverhalten in Dekantierzentrifugen. Ph.D. Thesis, Universität Karlsruhe (TH), Germany, 2006.
[56] M. Sambuichi, H. Nakakura, K. Osasa, Zone settling of concentrated slurries in a centrifugal field, J. Chem. Eng. Jpn 24 (4) (1991) 489–494.
[57] T. Detloff, T. Sobisch, D. Lerche, Particle size distribution by space or time dependent extinction profiles obtained by analytical centrifugation (concentrated systems), Powder Technol. 174 (1–2) (2007) 50–55.
[58] A.D. Stickland, Solid-Liquid Separation in the Water and Wastewater Industries. Ph.D. Thesis, The University of Melbourne, Australia, 2005.
[59] H. Reinach, Gleichgewicht und Kinetik der Pressentfeuchtung im Zentrifugalfeld einer Becherzentrifuge und in einer Stempelpresse, dargestellt an einem stark kompressiblen Schlamm. Ph.D. thesis, University of Karlsruhe (TH), Germany, 1992.
[60] W.H. Stahl, Fest-Flüssig-Trennung. 2, Industrie-Zentrifugen; Maschinen- & Verfahrenstechnik, DrM Press, Männedorf, Switzerland, 2004.
[61] H.K. Baust, H. Nirschl, M. Gleiß, Resolved simulation for the prediction of classification in decanter centrifuges, Chem. Eng. 8 (2024) 48.